Physics and Astronomy Faculty Research Publications

Physics and Astronomy

2-1-2009

A Deep *XMM-Newton* Observation of the Quasar 3C 287

G. Salvesen
University of Michigan

J. M. Miller
University of Michigan

E. Cackett
University of Michigan, ecackett@wayne.edu

A. Siemiginowska
Harvard-Smithsonian Center for Astrophysics

A DEEP *XMM-NEWTON* OBSERVATION OF THE QUASAR 3C 287

G. SALVESEN[1], J. M. MILLER[1], E. CACKETT[1,3], AND A. SIEMIGINOWSKA[2]
[1] Department of Astronomy, The University of Michigan, 500 Church Street, Ann Arbor, MI 48109-1042, USA; salvesen@umich.edu, jonmm@umich.edu
[2] Harvard-Smithsonian Center for Astrophysics, 60 Garden Street, Cambridge, MA 02138, USA; aneta@head.cfa.harvard.edu

ABSTRACT

We report on an *XMM-Newton* observation of the $z = 1.055$ quasar and Gigahertz Peaked Spectrum (GPS) source 3C 287. Our 62.3 ks observation provides an exceptional X-ray view of a prominent member of this important subclass of active galactic nuclei (AGNs). The X-ray spectra of 3C 287 are consistent with a simple absorbed power law with a spectral index of $\Gamma = 1.72 \pm 0.02$. Our fits imply a bolometric luminosity of $L = 5.8 \pm 0.2 \times 10^{45}$ erg s^{-1} over the 0.3–10.0 keV band; this gives a mass lower limit of $M_{\rm BH\,min} \geqslant 4.6 \times 10^7\ M_\odot$ assuming X-rays contribute 10% of the bolometric luminosity and radiation at the Eddington limit. Iron emission lines are common in the X-ray spectra of many AGNs, but the observed spectra appear to rule out strong emission lines in 3C 287. The simple power-law spectrum and the absence of strong emission lines may support a picture where our line of sight intersects a relativistic jet. Milliarcsecond radio imaging of 3C 287 appears to support this interpretation. We discuss our results in the context of different AGNs subclasses and the possibility that GPS sources harbor newly formed black hole jets.

Key words: accretion, accretion disks – black hole physics – relativity

1. INTRODUCTION

Connections between accretion disks and relativistic jets in black hole systems are theoretically anticipated, but observational constraints on this coupling remain elusive. Some progress has been made by tracking X-ray and radio flux variations in stellar-mass black holes, for instance, where transient outbursts evolve over weeks and months (e.g., Gallo et al. 2003). However, observations of stellar-mass black holes average over vastly more dynamical timescales and much larger regions than observations of the supermassive black holes powering active galactic nuclei (AGNs). In a sense, every observation is an average, and every image is coarse.

Gigahertz Peaked Spectrum (GPS) sources and Compact Steep-Spectrum (CSS) sources are well known AGNs subclasses. Beyond the flux-based criteria used to separate these classes, surveys reveal an important size difference: GPS sources are generally less than 1 kpc in projected linear size, while CSS sources can be 20 times larger (see, e.g., Edwards & Tingay 2004). These small size scales imply relatively young jets from new activity. Compact Symmetric Objects (CSOs)—a subclass of GPS and CSS sources—represent an even more interesting regime in which to explore disk–jet connections. Proper motion studies of some CSO sources imply jets that have only become active within the last 10^3 years (Conway 2002).

3C 287 is a well known radio-loud quasar at $z = 1.055$ that falls into the GPS category, and perhaps also into the CSO category (Kellerman et al. 1998). Our preliminary analysis of a prior *Chandra* observation suggested the presence of a broad, relativistic iron diskline. Such lines are excellent probes of the inner disk (e.g., Miller 2007), making 3C 287 an even more exciting target in which to explore accretion flows and to study disk–jet connections. GPS quasars do not necessarily have the same X-ray properties as GPS galaxies. GPS galaxies show large X-ray absorption columns, while GPS quasars show significantly less absorption (Siemiginowska et al. 2008). X-ray absorption in GPS galaxies may result from an orientation coincident with an obscuring "torus," possibly blocking the

central engine from direct observation (Guainazzi et al. 2006). Although a modest survey of GPS sources has been performed with *Chandra* (Siemiginowska et al. 2003, 2008), deep X-ray observations of these sources are rare.

In the following sections, we report the results of fits to the spectra of 3C 287 as measured using the *XMM-Newton* EPIC/pn, MOS-1, MOS-2, and OM cameras. Fits to these spectra suggest power-law behavior typical of CSS sources and the absence of strong Fe K emission lines. We discuss these results as well as their implications on emission mechanisms and our line of sight to 3C 287.

2. OBSERVATIONS AND DATA REDUCTION

XMM-Newton observed 3C 287 for a total of 62.3 ks, starting on 2006 July 19 at 01:57:09 (UT). The EPIC/pn and MOS cameras were run in "PrimeFullWindow" mode with the "medium" optical blocking filter. The RGS was run in the standard "spectroscopy" mode. The OM obtained a sequence of images in *V* (corresponding to UV in the source frame) in order to sample any light from an accretion disk. The results reported in this analysis are restricted to the EPIC cameras and to the OM; the RGS spectra are count-limited and do not add much information.

SAS version 7.1 was used to reduce and filter the data and create products from the raw ODF files. The tasks *epproc*, *emproc*, and *omichain* were used to create calibrated event lists from the pn, MOS, and OM cameras. Subsequent reduction was performed using "xmmselect." The pn event list was filtered to accept only good events (via "PATTERN ⩽ 4" and "FLAG = 0"). The MOS event lists were also filtered to accept only good events (via "PATTERN ⩽ 12" and "FLAG = 0").

Inspection of the EPIC light curves revealed strong flaring at the end of the observation; therefore, only the first 48.1 ks of the pn exposure was used to create images and spectra, and only the first 53.8 ks of the MOS exposures were used. Circles with radii of 30″ centered on 3C 287 were used as source extraction regions. Background regions of equivalent size were taken nearby to the source, on the same CCD. The pn source and background spectra were generated by grouping channels 0–20,479 by a factor of 5; the MOS spectra were generated by
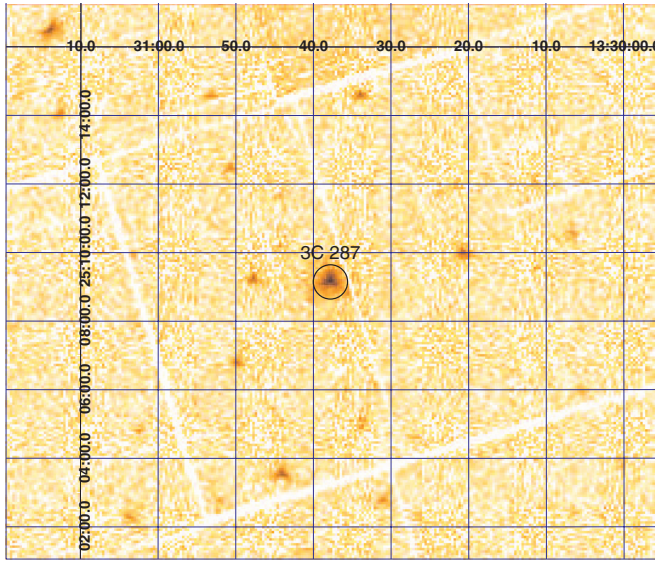
---

[3] Dean McLaughlin Fellow.

Figure 1. EPIC/MOS-2 X-ray image (0.3–10.0 keV) of 3C 287. The source is circled.

grouping channels 0–11,999 by a factor of 15. Custom response files for the EPIC spectra were generated using the tools *rmfgen* and *arfgen*.

To ensure valid constraints from the use of the χ^2 fitting statistic, the EPIC spectra were binned to require at least 20 counts per bin using the FTOOL *grppha*. Spectra were then fitted using XSPEC version 11.3.2 (Arnaud 1996). All EPIC spectra were fitted in the 0.3–10.0 keV band as the cameras are best calibrated in this range. All errors in this work are 90% confidence errors as derived using the XSPEC "error" command, unless otherwise noted.

3. ANALYSIS AND RESULTS

3.1. EPIC Analysis

Model spectra were fitted to the data. The pn and MOS spectral data were fitted jointly, allowing an overall normalization constant to float between the spectra. This normalization constant was within 3% of unity. All models were multiplied by the XSPEC model "phabs" to account for photoelectric absorption by neutral hydrogen along the line of sight, assuming default abundances. The X-ray spectra were jointly fitted using simple power-law models, where χ^2 statistics determined the goodness of each fit. The three models we report are spectral fits to a power law, broken power law, and line functions incorporated into the power law. We added line functions to the power-law model over a restricted energy range of 3.1–3.4 keV which is where we expect to locate an Fe K emission line based on a redshift of $z = 1.055$ for 3C 287. Spectral parameter values and fluxes, along with the corresponding upper limits, are recorded for fits to each of the models. Investigation of our orientation relative to the jet or disk comes from equivalent width methods, determined by the upper limit of the normalization for the line functions. Both narrow and broad line fits were made to ensure robust limits on the equivalent width.

We present images as observed by *XMM-Newton* and spectral fits along with parameters obtained using XSPEC. Figures 1 and 2 show an X-ray and *V*-band image of 3C 287, respectively, as observed by *XMM-Newton*. The results from the joint fits of MOS-1 and MOS-2 spectra to the pn spectra of 3C 287 over the 0.3–10.0 keV energy band are listed in Table 1.
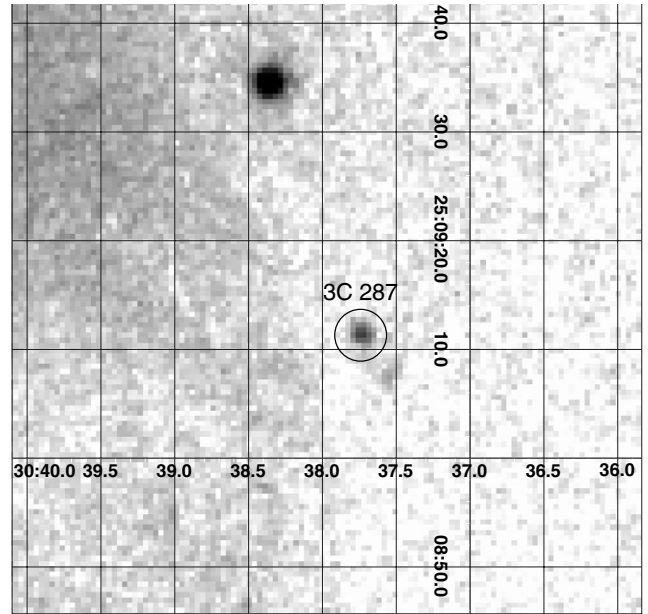

Figure 2. OM *V*-band image of 3C 287, generated from a single exposure. The source was found to have a *V* magnitude of 18.2. The apparent diffuse emission feature in the upper left corner is likely instrumental and has negligible impact on our OM measurements.

Both a simple power-law model and power law with a break in the 0.3–10.0 keV range yield acceptable fits based on χ^2 statistics. The best-fit power-law model gives $\chi^2/\nu = 650.3/598 = 1.09$, where ν is the number of degrees of freedom. The best-fit broken power-law model result is $\chi^2/\nu = 643.4/596 = 1.08$; this is not a statistically significant improvement over the simple power-law model. Spectral fits using a power-law model are shown in Figure 3. The simple power-law model gives a flux of $F = 7.1 \pm 0.2 \times 10^{-13}$ erg cm^{-2} s^{-1} over the 0.3–10.0 keV band. We calculate a corresponding bolometric luminosity of $L = 5.8 \pm 0.2 \times 10^{45}$ erg s^{-1} based on the stated redshift $z = 1.055$, allowing us to place a minimum mass estimate on the central engine. The lower mass limit of 3C 287 is $M_{\rm BH\,min} \geqslant 4.6 \times 10^7\, M_\odot$, assuming that the X-ray luminosity accounts for 10% of the bolometric luminosity and radiation at the Eddington luminosity limit. We calculate a recession velocity of $v_{\rm rec} = (0.62)c$ from the redshift, corresponding to a distance of $d = 2.6$ Gpc assuming $H_0 = 71$ km s^{-1} Mpc^{-1}. This is the distance we assume when calculating the luminosity.

An interesting feature in the power-law model joint fits is the absence of a strong Fe K emission line centered at a rest-frame energy of 6.4 keV. Figure 3 plots spectra in the observed frame. Due to redshift, we expect to search for the presence of this line at 3.1 keV. Jointly fitting the spectra of three simultaneous observations of 3C 287 with *XMM-Newton*'s EPIC/pn, MOS-1, and MOS-2 appears to exclude a very strong Fe K emission line. We investigate the possibility of a narrow to broad emission line within the rest-frame energy range of 6.4–6.97 keV. Freezing the width of a Gaussian profile to zero in the fit placed a narrow line upper limit of 69 eV on the equivalent width. We find a broad line upper limit of 312 eV using the XSPEC model "diskline" instead of fitting a broad Gaussian line profile to account for the possibility of a relativistically broadened diskline. However, the limits on the narrow line, which is expected to come from a large region, could indicate that the innermost accretion flow may not be directly observed. This is consistent with the compact size of the radio-emitting region and supports the conclusion
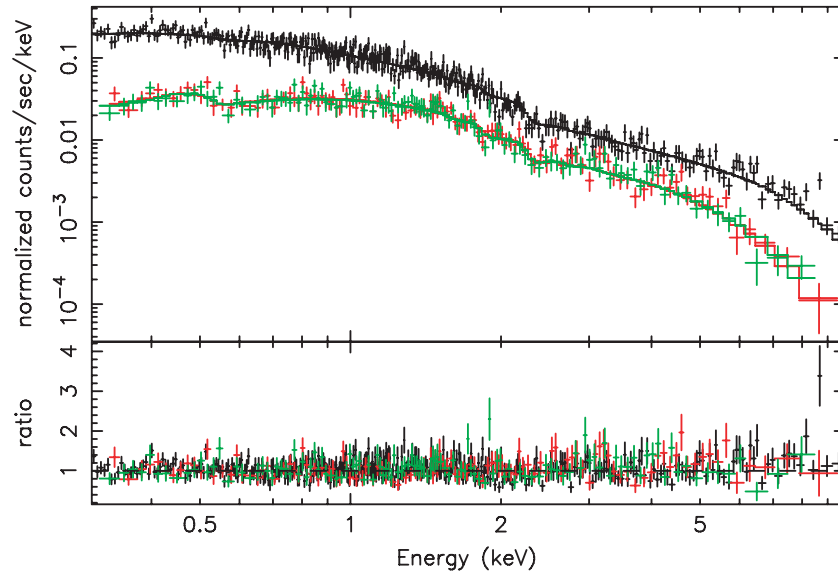
Figure 3. *XMM-Newton* X-ray spectra of 3C 287 (black: pn; red: MOS-1; blue: MOS-2). Energy units are shown in the observed frame. The spectra were fitted with a simple absorbed power-law model. The spectra themselves and the data/model ratio indicate that no strong emission or absorption lines are present.

Table 1
Spectral Fit Parameters

Model Parameter	EPIC/pn
Power-Law Model	
N_H (10^{19} cm^{-2})	< 3.1
Γ	1.72 ± 0.02
Norm. (10^{-4} ph cm^{-2} s^{-1})	1.04 ± 0.02
χ^2/ν	$650.3/598 = 1.09$
Flux (10^{-13} erg cm^{-2} s^{-1})	7.1 ± 0.2
Lumin. (10^{45} erg s^{-1})	5.8 ± 0.2
Broken Power-Law Model	
N_H (10^{19} cm^{-2})	< 18
Γ_1	1.74 ± 0.09
Γ_2	1.5 ± 0.2
E_{break} (keV)	4.1 ± 0.3
Norm. (10^{-4} ph cm^{-2} s^{-1})	1.04 ± 0.06
χ^2/ν	$643.4/596 = 1.08$
Flux (10^{-13} erg cm^{-2} s^{-1})	7.3 ± 0.5
Lumin. (10^{45} erg s^{-1})	5.9 ± 0.5
Line Profile Fits to Power-Law Model	
(narrow line) : (broad line)	
N_H (10^{19} cm^{-2})	< 3.5 : < 3.7
Γ	$1.73 \pm 0.02 : 1.72 \pm 0.03$
Norm.$_{Power-Law}$ (10^{-4} ph cm^{-2} s^{-1})	$1.04 \pm 0.02 : 1.04 \pm 0.02$
E_{line} (keV)	3.2 : 3.1
Norm.$_{Line}$ (10^{-6} ph cm^{-2} s^{-1})	< 1.0 : < 4.3
χ^2/ν	$644.9/594 = 1.09 : 645.5/592 = 1.09$
Flux (10^{-13} erg cm^{-2} s^{-1})	$7.1 \pm 0.2 : 7.1 \pm 0.3$
Lumin. (10^{45} erg s^{-1})	$5.8 \pm 0.1 : 5.7 \pm 0.3$
EW (eV)	69 : 312

Notes. The results of joint spectral fits to the EPIC/pn, MOS-1, and MOS-2 spectra of 3C 287 are detailed above. Though a broken power law provides a slightly better fit, the spectrum is consistent with a simple power-law form. The narrow line is fitted with a Gaussian model, while the broad line is fitted with a diskline model. Upper limits are given for the column density of neutral gas along the line of sight and for line profile normalizations. The bolometric luminosity is quoted in the table assuming that X-rays contribute 10% of the bolometric luminosity. We report the best-fit X-ray flux values over the 0.3–10.0 keV band. Reported flux and luminosity of 3C 287 in the text are taken from the power-law fits.

that a relativistically broadened iron line is not present. The limits on narrow line emission are typical for Seyfert-1 AGNs (Nandra et al. 1997). The limits are less constraining when viewed in the context of high-luminosity objects (see Bianchi et al. 2007), though there is considerable scatter in the strength of iron emission lines in such sources.

3.2. OM Analysis

To obtain a preliminary characterization of the broadband spectral energy distribution, we focused on a single characteristic OM exposure, frame 433. The OM *V* filter has a central wavelength of 5430 Å and spans roughly 1000 Å. The task *omichain* generates a list of source detections; 3C 287 was detected at the 12σ level of confidence, as imaged in Figure 2. A count rate of 0.7 ± 0.1 counts s^{-1} was recorded. The measured instrumental magnitude is $V = 18.2 \pm 0.2$. Using the recipe on the SAS web site appropriate for blue continuum sources, the count rate given above can be converted to a flux of $1.0 \pm 0.1 \times 10^{-12}$ erg cm^{-2} s^{-1}.

3.3. Broadband Analysis

To place the X-ray flux trends from 3C 287 in context, we constructed a broadband spectral energy distribution using XSPEC. Using the ftool "flx2xsp" we generated single-bin spectral files. To make use of this tool, the flux in the bin is required, as well as the bin boundaries. The OM *V* filter spans approximately 1000 Å. The Two Micron All Sky Survey (2MASS) recorded *J* and *H* magnitudes of 16.44 and 16.06, respectively. These magnitudes were converted into fluxes using the *Spitzer* Science Center conversion tool, and then into spectral files using the filter boundaries appropriate to the 2MASS *J* and *H* filters (Cutri et al. 2003). Very Large Array (VLA) observations of 3C 287 recorded a flux density of 3.22 Jy at 5 GHz (Kellermann et al. 1998). We also converted this flux into a spectral file. For visual clarity, fiducial flux errors of 10% were assumed for the *J*, *H*, and radio fluxes, though true statistical errors are far lower.

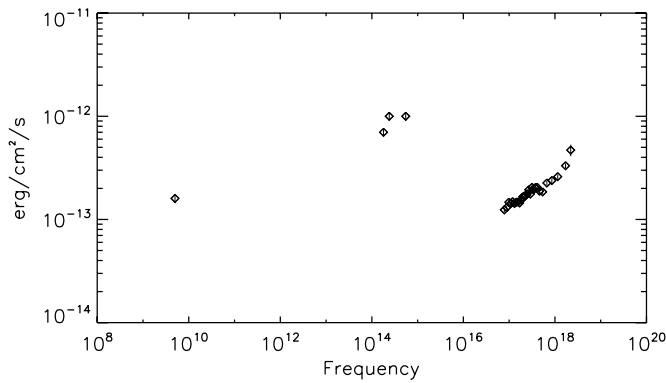The resulting broadband spectral energy distribution of 3C 287 is shown in Figure 4. The emission of 3C 287 peaks

Figure 4. Broadband spectral energy distribution of 3C 287. X-ray and optical points are from our *XMM-Newton* observations. Infrared points are from 2MASS observations in *J* and *H*. The single radio point is from a VLA observation at 5 GHz.

in the *H*, *J*, and UV bands in the observed frame, or the optical and UV bands in the source frame. Thus, we do observe the "Big Blue Bump" emission that is usually seen in radio-quiet quasars and interpreted as thermal emission from an accretion disk (Shields 1978). The OM measured luminosity is about 6×10^{45} erg s^{-1} and it indicates high accretion rates in this system.

The radio to X-ray luminosity ratio is smaller than typically observed in samples of radio-loud sources (blazars: Fossati et al. 1998; FRI galaxies: Donato et al. 2004; FRII-type radio-loud quasars and galaxies: Evans et al. 2006; Belsole et al. 2006; Balmaverde et al. 2006) in terms of the source being more powerful in radio than a typical radio-loud quasar (Elvis et al. 1994; Richards et al. 2006). However, the ratio agrees with the ratios observed in compact radio sources (GPS galaxies: Guainazzi et al. 2006; Vink et al. 2006; GPS/CSS quasars: Siemiginowska et al. 2008). In the case of GPS quasars the X-ray emission could originate in a jet via Inverse Compton scattering of the IR photons on the relativistic electrons in a parsec scale jet (Błażejowski et al. 2004). This emission could contribute to the observed X-ray emission.

We also calculate the α_{ox} parameter (Avni & Tananbaum 1982) usually used to characterize a relative strength of the optical–UV thermal disk emission and the Comptonized X-ray component (for example, Sobolewska et al. 2004). This parameter is defined as $\alpha_{ox} = \log[\text{Flux}(2500\ \text{Å})/\text{Flux}(2\ \text{keV})]/2.605$ in the source rest frame. We take the *V*-band magnitude and assume a spectral slope of $f_\nu = \nu^{-0.5}$ to calculate the flux at the rest-frame $\lambda = 2500$ Å and the measured *XMM* flux at 2 keV. Our α_{ox} is equal to 1.7. It is in the high end of a typical distribution of the α_{ox} parameter for radio-quiet quasars ($\alpha_{ox} = 1.5 \pm 0.2$, Kelly et al. 2008) and also radio-loud quasars (Bechtold et al. 1994).

4. DISCUSSION AND CONCLUSIONS

In the above sections, we have detailed our analysis of a deep exposure of 3C 287 made with *XMM-Newton*. In the 0.3–10.0 keV observed frame (approximately 0.6–20 keV in the source frame), the spectrum is well represented by a simple absorbed power-law model. In AGNs that are viewed at a modest inclination, it is common to observe either an X-ray warm absorber (likely a disk wind; see, e.g., Reynolds 1997) or a soft excess (perhaps also tied to the disk; e.g., Crummy et al. 2006), and an Fe K emission line due to hard X-ray illumination

of the disk, the torus, or both. Fits made with a broken power law were made in order to test for evidence of either a soft excess or warm absorption at low energy. However, these fits do not provide a significantly improved description of the data. Similarly, fits with Gaussian and diskline functions place limits on the strength of both narrow and broad emission lines.

It is also worth noting that our results place a limit of approximately 5×10^{19} atoms cm^{-2} on any neutral absorbing gas along our line of sight to 3C 287. This limit is about a factor of 2 lower than the measurement reported by Siemiginowska et al. (2003). Although models where the source is confined by dense gas (Snellen et al. 2000; Alexander 2000) have not been completely ruled out, new work argues against confinement (Guainazzi et al. 2004; Morganti 2008).

Our X-ray results are consistent with emission related to a jet that dominates over the typical X-ray emission associated with the accretion process. The emission we observe could be accounted for through a combination of synchrotron and synchrotron self-Comptonization in the jet, hot spots, and compact lobes.

A line of sight coincident with the jet is suggested by deep milliarcsecond radio imaging of 3C 287. Very Long Baseline Array imaging at 15 GHz reveals an extremely compact core in 3C 287, with a minimal extension of less than 4 milliarcseconds, or less than about 20 pc in the source frame (Kellermann et al. 1998). This core is among the smallest and least extended in the survey of AGNs conducted by Kellerman et al. (1998), and is strongly suggestive of a jet that lies primarily along our line of sight. In many AGNs, the presence of a strong, narrow iron fluorescence line is tied to X-ray irradiation of a parsec-scale torus (e.g., Antonucci 1993; Urry & Padovani 1995; Yaqoob & Padmanabhan 2004; Nandra 2006). Thus, although the radio core is remarkably small by the standards of jet sources, it is still large enough to block our line of sight to the innermost region (or even the torus) in 3C 287. A possible difficulty with this interpretation is that emission consistent with the Big Blue Bump is observed. This may indicate that the jet does not block all of the disk emission along our line of sight.

The question arises, then, why extreme blazar-like variability is not observed in 3C 287 (and similar sources). A partial answer may lie in the likely nature of CSS and GPS sources. Proper motion studies of some sources in this class suggest that these AGNs have only been powering jets for approximately 10^3 years (Conway 2002); however, a young radio source may have higher efficiency of converting the jet power into radiation. In such young sources the X-ray emission may originate in compact lobes and hot spots (Stawarz et al. 2008) if the line of sight is not aligned directly with a jet. In this model there is no expectation of the X-ray variability typically observed in blazars. Note that there is no change in X-ray luminosity between the *Chandra* and *XMM-Newton* observations (Siemiginowska et al. 2008).

The broadband spectral energy distribution shown in Figure 4 may further support this interpretation. The source is more radio-loud than typical radio-loud quasars (Elvis et al. 1994; Richards et al. 2006; Siemiginowska et al. 2008), while its X-ray emission is relatively weak with $\alpha_{ox} = 1.7$. This suggests a weak contribution from the standard emission component (for example, a parsec scale jet; Błażejowski et al. 2004) observed in radio-loud quasars.

We conclude that 3C 287 may be a "proto-blazar" candidate. Dedicated multiwavelength monitoring of sources like 3C 287 over a period of years can help to better reveal the nature of this source.

REFERENCES

Alexander, P. 2000, MNRAS, 319, 8
Antonucci, R. 1993, ARA&A, 31, 473
Arnaud, K. A. 1996, in ASP Conf. Ser. 101, ADASS V, ed. G. Jacoby & J. Barnes (San Francisco, CA: ASP), 17
Avni, Y., & Tananbaum, H. 1982, ApJ, 262, L17
Balmaverde, B., Capetti, A., & Grandi, P. 2006, A&A, 451, 35
Bechtold, J., et al. 1994, AJ, 108, 374
Belsole, E., Worrall, D. M., & Hardcastle, M. J. 2006, MNRAS, 366, 339
Bianchi, S., Guainazzi, M., Matt, G., & Fonseca Bonilla, N. 2007, A&A, 467, L19
Błażejowski, M., Siemiginowska, A., Sikora, M., Moderski, R., & Bechtold, J. 2004, ApJ, 600, L27
Conway, J. E. 2002, New Astron. Rev., 46, 263
Crummy, J., Fabian, A. C., Gallo, L., & Ross, R. R. 2006, MNRAS, 365, 1067
Cutri, R. M., et al. 2003, The IRSA 2MASS All-Sky Survey Point Source Catalog, NASA/IPAC Infrared Science Archive (http://irsa.ipac.caltech.edu/applications/Gator/)
Donato, D., Sambruna, R. M., & Gliozzi, M. 2004, ApJ, 617, 915
Edwards, P. G., & Tingay, S. J. 2004, A&A, 424, 91
Elvis, M., et al. 1994, ApJS, 95, 1
Evans, D. A., et al. 2006, ApJ, 653, 1121

Fossati, G., Maraschi, L., Celotti, A., Comastri, A., & Ghisellini, G. 1998, MNRAS, 299, 433
Gallo, E., Fender, R., & Pooley, G. G. 2003, MNRAS, 344, 60
Guainazzi, M., Siemiginowska, A., Rodriguez-Pascual, P., & Sgnhellini, C. 2004, A&A, 421, 461
Guainazzi, M., Siemiginowska, A., Stanghellini, C., Grandi, P., Piconcelli, E., & Azubike Ugwoke, C. 2006, A&A, 446, 87
Kellermann, K. I., et al. 1998, ApJ, 115, 1295
Kelly, B. C., Bechtold, J., Trump, J. R., Vestergaard, M., & Siemiginowska, A. 2008, ApJS, 176, 355
Miller, J. M. 2007, ARA&A., 45, 441
Morganti, R. 2008, in ASP Conf. Ser. 386, Extragalactic Jets: Theory and Observation from Radio to Gamma-Ray, ed. T. A. Rector & D. S. De Young (San Francisco, CA: ASP), 210
Nandra, K. 2006, MNRAS, 368, L62
Nandra, K., George, I. M., Mushotzky, R. F., Turner, T. J., & Yaqoob, T. 1997, ApJ, 477, 602
Reynolds, C. S. 1997, MNRAS, 286, 513
Richards, G. T., et al. 2006, ApJS, 166, 470
Shields, G. A. 1978, Nature, 272, 706
Siemiginowska, A., LaMassa, S., Aldcroft, T. L., Bechtold, J., & Elvis, M. 2008, ApJ, 684, 811
Siemiginowska, A., et al. 2003, PASA, 20, 113
Snellen, I. A. G., Schilizzi, R. T., Miley, G. K., de Bruyn, A. G., Bremer, M. N., & Rottgering, H. J. A. 2000, MNRAS, 319, 445
Sobolewska, M. A., Siemiginowska, A., & Zycki, P. T. 2004, ApJ, 608, 80
Stawarz, L., Ostorero, L., Begelman, M. C., Moderski, R., Kataoka, J., & Wagner, S. 2008, ApJ, 680, 911
Urry, C. M., & Padovani, P. 1995, PASP, 107, 803
Vink, J., Snellen, I., Mack, K.-H., & Schilizzi, R. 2006, MNRAS, 367, 928
Yaqoob, T., & Padmanabhan, U. 2004, ApJ, 604, 63